Measurement of neutron detection efficiencies in NaI using the Crystal Ball detector

T.D.S. Stanislaus[a], D.D. Koetke[a,*], C. Allgower[c,1], V. Bekrenev[l], K. Benslama[m], E. Berger[j], W.J. Briscoe[g], M. Clajus[j,2], J.R. Comfort[d], K. Craig[d], A. Gibson[a], D. Grosnick[a,3], G.M. Huber[m], D. Isenhower[b], T. Kasprzyk[d], N. Knecht[m], A. Koulbardis[l], N. Kozlenko[l], S. Kruglov[l], T. Kycia[e,4], G.J. Lolos[m], I. Lopatin[l], D.M. Manley[i], R. Manweiler[a], A. Marusic[j,n,5], S. McDonald[j,6], B.M.K. Nefkens[j], J. Olmsted[i], Z. Papandreou[m], D. Peaslee[k], R.J. Peterson[f], N. Phaisangittisakul[j], M. Pulver[j], A.F. Ramirez[d], M. Sadler[b], A. Shafi[g], I. Slaus[n], H. Spinka[c], A. Starostin[j,l], H.M. Staudenmaier[h], I. Supek[n], J. Thoms[a], W.B. Tippens[j,7]

[a] *Neils Science Center, Department of Physics and Astronomy, Valparaiso University, Valparaiso, IN 46383, USA*
[b] *Abilene Christian University, Abilene, TX 79699, USA*
[c] *Argonne National Laboratory, Argonne, IL 60439, USA*
[d] *Arizona State University, Tempe, AZ 85287, USA*
[e] *Brookhaven National Laboratory, Upton, NY 11973, USA*
[f] *University of Colorado, Boulder, CO 80309, USA*
[g] *George Washington University, Washington, DC 20052, USA*
[h] *Universitat Karlsruhe, Karlsruhe, Germany 76128*
[i] *Kent State University, Kent, OH 44242, USA*
[j] *University of California, Los Angeles, Los Angeles, CA 90095, USA*
[k] *University of Maryland, College Park, MD 20742, USA*
[l] *Petersburg Nuclear Physics Institute, Gatchina, Leningrad, Russia 188350*
[m] *University of Regina, Regina, Saskatchewan, Canada S4S 0A2*
[n] *Rudjer Boskovic Institute, Zagreb, Croatia 100000*

Abstract

We report on a measurement of the neutron detection efficiency in NaI crystals in the Crystal Ball (CB) detector obtained from a study of $\pi^- p \to \pi^0 n$ reactions at the Brookhaven National Laboratory AGS. A companion

*Corresponding author. Tel.: +1-219-464-5377; fax: +1-219-464-5489.

E-mail address: donald.koetke@valpo.edu (D.D. Koetke).

[1] Present Address: Indiana University Cyclotron Facility, Bloomington, IN 47408, USA.

[2] Present Address: NOVA R&D, Inc., Riverside, CA 92507, USA.

[3] Present Address: Ball State University, Muncie, IN 47306, USA.

[4] Deceased.

[5] Present Address: Brookhaven National Laboratory, Upton, NY 11973, USA.

[6] Present Address: TRIUMF, Vancouver, BC, Canada V6T 2A3.

[7] Present Address: Nuclear Physics Division, U.S. Department of Energy, Germantown, MD 20874, USA.

GEANT-based Monte Carlo study has been done to simulate these reactions in the CB, and a comparison with the data is provided. © 2001 Elsevier Science B.V. All rights reserved.

PACS: 29.40.Vj; 29.85.+c; 28.20.−v

Keywords: Neutron efficiency in NaI; Neutrons in GEANT

1. Introduction

The Crystal Ball (CB) collaboration is engaged in a program to study π^-p and K$^-$p interactions that result in final states consisting of particles that are all charge-neutral. As the name implies, we have used the CB detector, built originally at SLAC for use with colliding e$^+$e$^-$ beams in SPEAR[1–4]. After four years of service in the DORIS rings at DESY [5–8], it was returned to SLAC and subsequently, in 1995, it was moved to the Brookhaven National Laboratory Alternating Gradient Synchrotron (BNL-AGS) to investigate baryon spectroscopy. After some detector refurbishing, which included upgrading the electronics and data acquisition systems and installing a liquid hydrogen target, our program of neutral hadron spectroscopy began at the AGS in 1997 with four weeks of engineering running, followed by approximately 1000 h of data collection with π^- and with K$^-$ beams of varying energies in 1998. The targets included liquid hydrogen, the empty cryo-flask, and solid targets of heavier nuclei.

In each of the π^-p and K$^-$p reactions being studied, the neutral final state consists of photons and one neutron. The presence of neutrons in the CB represents a new pattern recognition challenge not frequently encountered in prior physics applications. A good understanding of the nature of the neutron interactions in NaI and the ability to simulate these interactions in Monte Carlo programs is of central importance to this research program. The lack of information in the literature on this subject has prompted the authors to undertake a detailed study of neutron interactions in the NaI crystals in the CB using the data collected during the 1997 and 1998 running periods. Moreover, the known problem of accu- rately simulating hadronic interactions moved us to examine the simulation of neutron interactions in the CB.

In the following sections, we present the results of this study. We have measured the absolute neutron detection efficiency in the CB as a function of the neutron energy. In parallel, we have used GEANT [9] to simulate π^-p and K$^-$p interactions in the CB detector with all neutral final-state particles. A comparison of these Monte Carlo generated neutron interactions with those of neutron interactions observed in the data is presented.

2. The detector

The experimental setup will be described in detail in a separate publication; only the most important components will be described here. The CB detector consists of 672 optically isolated NaI crystals, forming an approximately spherical shell, with each crystal viewed by a photomultiplier tube. A drawing of the CB detector is shown in Fig. 1. The NaI crystals are truncated triangular pyramids, which have a surface area of 11.1 cm^2 on the inner face 25.3 cm from the CB center. The NaI crystal length of 40.7 cm is 15.7 radiation lengths for the photons of interest in our studies. There are openings diametrically across the ball for the beam to enter and exit.

The target used for this study was a 10-cm-long by 10-cm-diameter cylindrical vessel filled with liquid hydrogen which was positioned at the center of the ball. The target was surrounded by a "veto barrel" formed of four plastic scintillation detec- tors, each a long segment of a cylinder. When the four scintillators were joined together they formed a cylinder positioned parallel to the axis of the
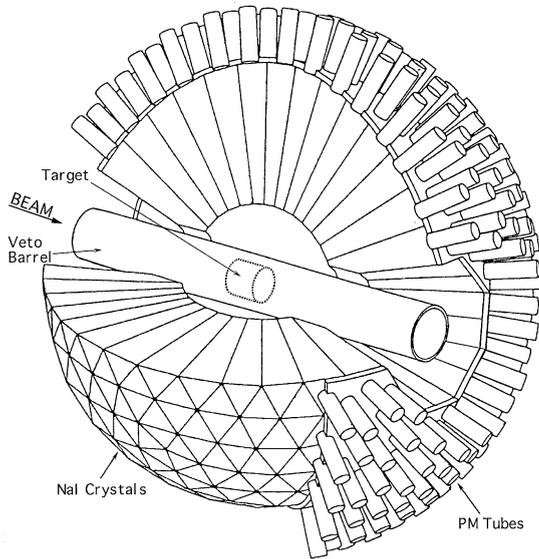
Fig. 1. A diagramatic representation of the CB is shown along with the veto barrel and the target. (The target is located inside the veto barrel.) The veto barrel is segmented into four sections along the cylinder axis with each section read out by photomultiplier tubes at both ends.

beam within the CB as shown in Fig. 1. This veto barrel extended to the entrance and exit holes in the CB. The veto barrel was employed in the trigger for the experiment to veto events when charged particles traversed the scintillators. This arrangement ensured that the energy deposited in the CB for a triggered event is due entirely to neutral particles coming from the production interaction or from the decay of neutral particles that travel only a short distance from their production.

Each crystal in the CB was energy calibrated. A 750 MeV/c π^- beam was used to produce the reactions $\pi^-p \to \pi^\circ n$ and $\pi^-p \to \eta n$. The energies of the two photons from the π° or the η decay were used to calculate the π° and η invariant mass, respectively. The calibration procedure adjusted the gain corrections of the 672 individual NaI crystals to optimize the centroid and the width of the π° and η invariant mass peaks. This method simultaneously aligns both the π° and the η invariant mass peaks to within $\sim 0.5\%$ of their accepted values.

3. Event selection

For this study of neutron interactions in the CB, we chose the charge exchange reaction (CEX) $\pi^-p \to \pi^\circ n$, where the π° decays to two photons. Because the momentum of the incident π^- was known and the interaction point was assumed to be at the center of the liquid hydrogen target, the direction and energy of the outgoing neutron were calculated using the two-body kinematics once the vector momentum of the π° was measured. To determine the neutron detection efficiencies, we used π^- beams whose momenta were 745, 720, 620, and 305 MeV/c. At 745 MeV/c, essentially the maximum π^- beam momentum available in the C6 line at the AGS, the most energetic neutrons from the CEX reaction emerged with ~ 420 MeV kinetic energy. (The radiative process $\pi^-p \to n\gamma$ has essentially the same maximum neutron energy.) In this report, we have limited our study to neutrons whose kinetic energies are $\leqslant 250$ MeV; above this value the number of events in our sample decreased dramatically because the forward-going neutrons disappear through the beam-exit opening and surrounding crystals.

The final state for the CEX reaction, if fully detected in the CB, appeared as three "clusters" of NaI crystals in which energy had been deposited: an electromagnetic shower from each of the two photons and a neutron-induced hadronic shower. Occasionally, the primary neutron scattered in a NaI crystal and the scattered neutron interacted in another NaI crystal producing an additional cluster. These four cluster events were also included in the analysis and, as seen in Table 1, occurred in $\sim 10\%$ of the events. In the CB analysis, a "cluster" is defined as 13 (or 12) adjacent NaI crystals surrounding and centered on the crystal with the largest deposited energy. To be included in the cluster, a NaI crystal was required to have a minimum deposited energy of 2 MeV. In some CEX reactions, one or more of these clusters was unobserved because a photon left through the beam-entrance or beam-exit opening in the CB, or because the neutron may have left through the beam exit opening or may have been undetected in the NaI. An event with less than two clusters was excluded from the sample because it would have

Table 1

a. Events remaining after cuts for the selection of CEX events (threshold = 20 MeV)			
Events with number of clusters >1	400640		
π°mass cut	120728		
π°opening angle $>30^\circ$	99347		
No crystals near beam openings in π° clusters	58996		
Missing mass of the π° is neutron mass	27729		
Predicted neutron is in the CB	14342		

b. Clusters per event			
	2 Clusters	3 Clusters	4 Clusters	> 4 Clusters
---	---	---	---	---
Predicted number of neutrons in CB	7854	5539	866	83
Neutron cluster does not overlap π° cluster	7746	4578	590	
Measured and predicted directions of neutron agree		4100	455	

insufficient information to reconstruct the CEX event for these studies. To be included in the list of observed clusters, a minimum energy (threshold) of 20 MeV was required to have been deposited in at least one NaI crystal in the cluster. (While a parallel study was done for a threshold energy of 10 MeV, all our results reported here are for a cluster threshold energy of 20 MeV unless explicitly noted below.) For each observed cluster, the total energy in the cluster was recorded, along with an optimized estimate of the particle direction between the primary interaction point and the cluster center. The cluster center was determined by an algorithm that weighted the individual NaI crystal positions by the energy detected in each crystal. From this information, the vector momentum of the particle that produced the cluster was calculated. Events in which the vector momenta for any two clusters were within 30° of each other were removed from the sample because the two clusters would likely share energy in an unknown way as clusters overlapped.

To reconstruct the vector momentum of the outgoing π°, each observed cluster was assumed to have been due to a photon interaction. The measured 4-momenta of these assumed photons were combined in pairs to calculate the invariant mass of the pair. Fig. 2 shows the invariant mass spectrum of all such combinations of two (photon) clusters giving clear evidence of a π° mass peak. Those invariant masses, which were not consistent with the π° mass, were due to a cluster pair that may have included a neutron interaction, or may
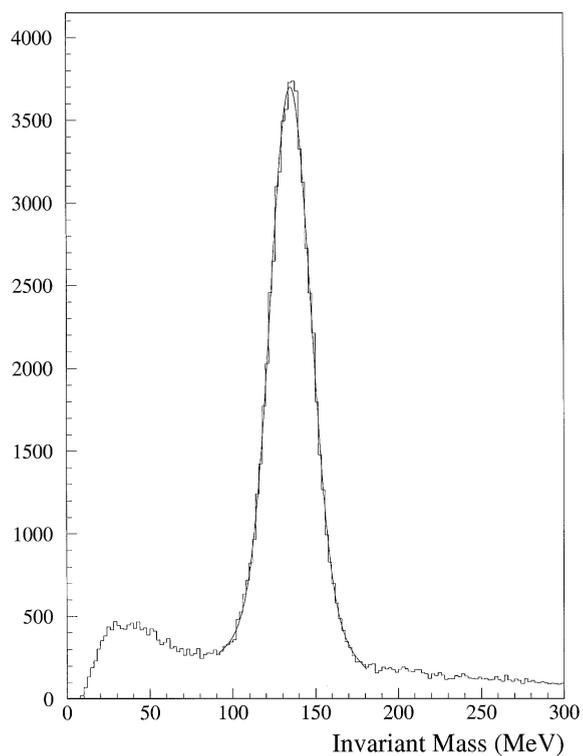

Fig. 2. The invariant mass of all two-photon clusters shows clear evidence for a π° mass peak on a continuous background. A Gaussian fit to the π° mass peak gives a FWHM of 29.4 MeV and a centroid of 134.6 MeV.

have arisen from a $\pi^- p \rightarrow \eta X$ interaction. Additional background came from other final states in which some photons exited through the beam-entrance or beam-exit openings in the CB. In those

relatively few events for which more than one combination of two clusters gave an invariant mass consistent with a π°, each π° was fully analyzed as described below.

In Fig. 3, we show the two-photon invariant mass spectrum for Monte Carlo simulated CEX events, which compares favorably with the corresponding two-photon invariant mass peak in Fig. 2 from our data. The FWHM of both peaks is 29.3 MeV, due in part to the assumption that the $\pi^- p$ interactions took place at the geometric center of the hydrogen target when, in fact, the $\pi^- p$ interaction points were distributed over the volume of the target.

For each π° event in Fig. 2, whose π° mass was in the range 110–160 MeV, we calculated the missing mass (MM) in the reaction $\pi^- p \rightarrow \pi^\circ X$, which we have plotted in Fig. 4. A clearly defined peak near the neutron mass is observed with a
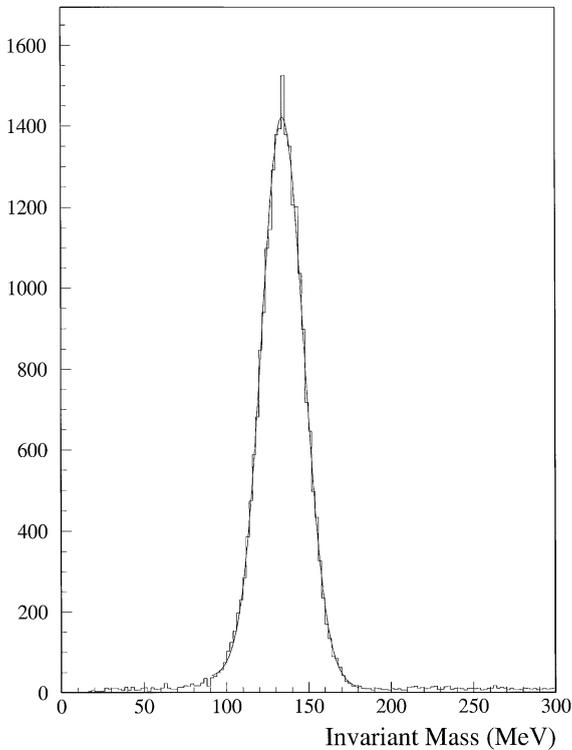

Fig. 4. The missing mass for the reaction $\pi^- p \rightarrow \pi^\circ X$ is shown here for all events from Fig. 2 whose π° invariant mass was in the range 110–160 MeV. Events in the peak within ± 50 MeV of the neutron mass were deemed to be consistent with the CEX reaction $\pi^- p \rightarrow \pi^\circ n$ and were therefore included in our sample for neutron studies in the Crystal Ball.

FWHM of 39 MeV. For all events in Fig. 2 whose MM is in the range 890 MeV $< \mathrm{MM} < 990$ MeV, i.e., broadly consistent with being a neutron, we have plotted the reconstructed π° momentum versus the reconstructed π° polar angle, measured with respect to the π^- beam direction in Fig. 5a. It is clear that these events are entirely consistent with the two-body kinematics associated with the CEX reaction ($\pi^- p \rightarrow \pi^\circ n$). The width of the band is a measure of our kinematic resolutions. For the same event sample shown in Fig. 5a, we have plotted the reconstructed π° mass in Fig. 5b. Comparison of this π° mass peak with that shown in Fig. 2 demonstrates how the cut on the neutron MM has selected the π° corresponding to the CEX reaction. For our neutron detection efficiency studies, an acceptable π° mass must fall in the range 119 MeV $\leqslant m_{\pi^\circ} \leqslant 151$ MeV, which is $\pm 1.5\sigma$.

Fig. 3. The invariant mass of two-photon clusters simulated in the GEANT-based Monte Carlo. The FWHM of the π° mass peak is 29.2 MeV with the centroid at 134.7 MeV, in good agreement with the fitted results shown in Fig. 2.
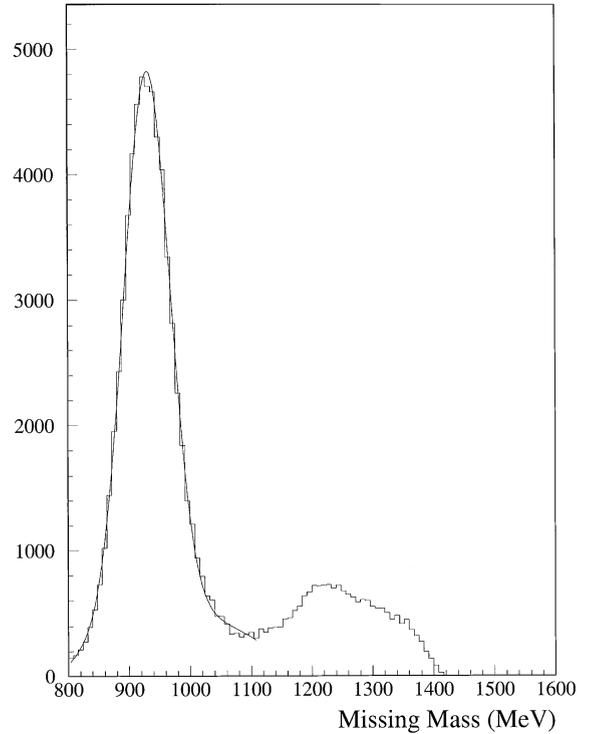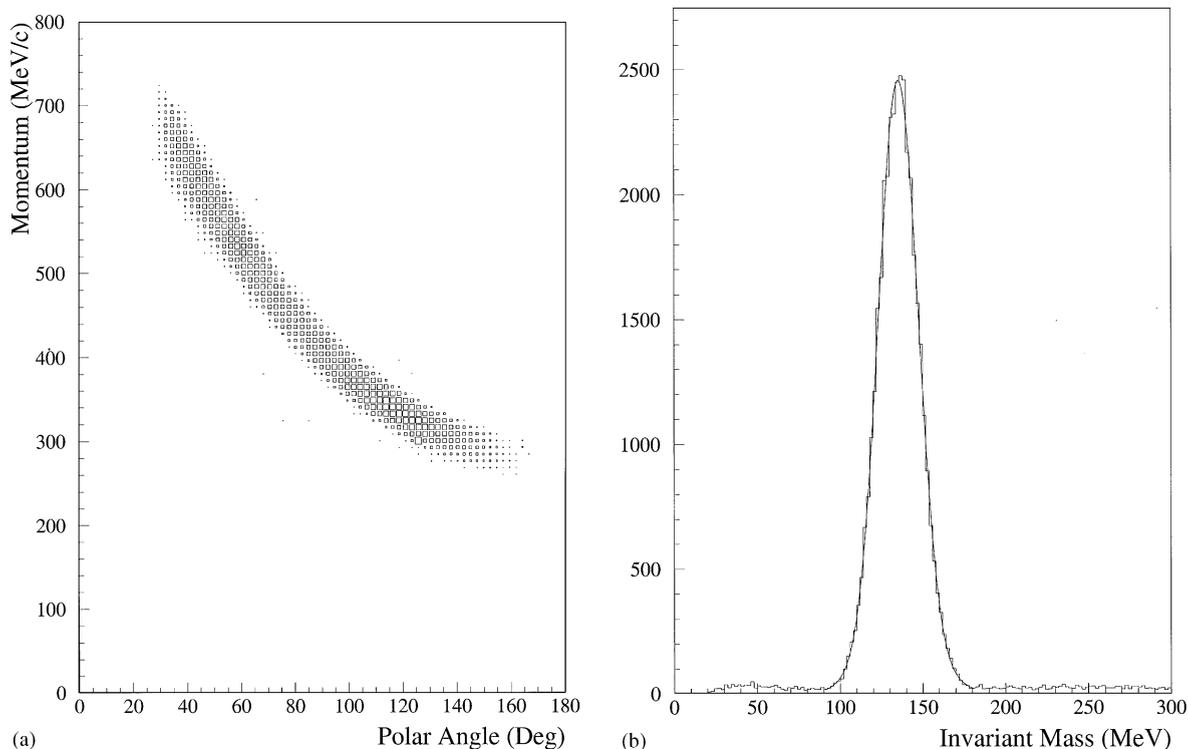
Fig. 5. For all events in Fig. 2, whose missing mass was within ± 50 MeV of the neutron mass, the reconstructed π° momentum is plotted versus its reconstructed polar angle in (a) showing the evident two-body kinematics for the CEX reaction. In (b) the π° mass is plotted for those events in Fig. 5a, showing a very small background under the π° mass peak. The CEX events used for neutron detection efficiencies had an invariant mass within $\pm 1.5\sigma$ of the π° mass.

In Fig. 5b there is a small, flat background whose magnitude under the π° mass peak (1–2% of the events in the peak) is consistent with the estimated number of background events under the neutron peak (890 MeV $<$ MM $<$ 990 MeV). These background events are either not CEX events or are CEX events in which a cluster is mis-identified, but which, given the kinematic information available, are unable to be separated from true CEX events and therefore, constitute a small contamination in our CEX sample.

The two-body kinematics also allowed us to calculate the expected polar and azimuthal angles (θ, ϕ) for the outgoing neutron once the vector momentum of the π° was known. Those events whose predicted angles for the outgoing neutron projected it out the beam-exit opening in the CB were removed from the analysis because the neutron could not have been detected in the CB.

If a cluster of NaI crystals with at least one crystal above the threshold energy was observed within $\pm 3\sigma$ of the predicted angles θ and ϕ, we assumed the cluster to have originated from neutron-induced hadronic interactions. In Fig. 6, we show the distribution of the differences between the predicted and the observed neutron polar and azimuthal angles for those events with three clusters. It is clear that cuts described above have retained events that are consistent with the assumed $\pi^- p \rightarrow \pi^\circ n$ reaction. The effects of the foregoing cuts on our event selection are shown in Table 1.

4. Neutron detection efficiency

The neutron detection efficiency in the CB was defined as the ratio of the number of observed
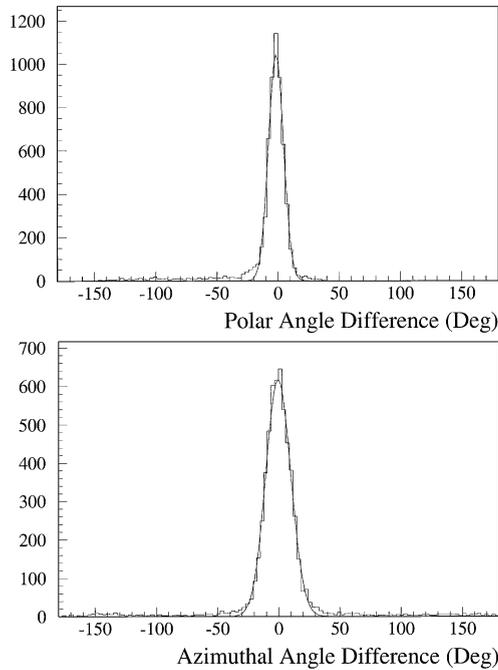
Fig. 6. For both polar and azimuthal angles, we show the distribution of the difference between the calculated and measured angles for the neutrons from the CEX reaction. Events were included in the analysis if the difference in both angles was less than $\pm 3\sigma$.
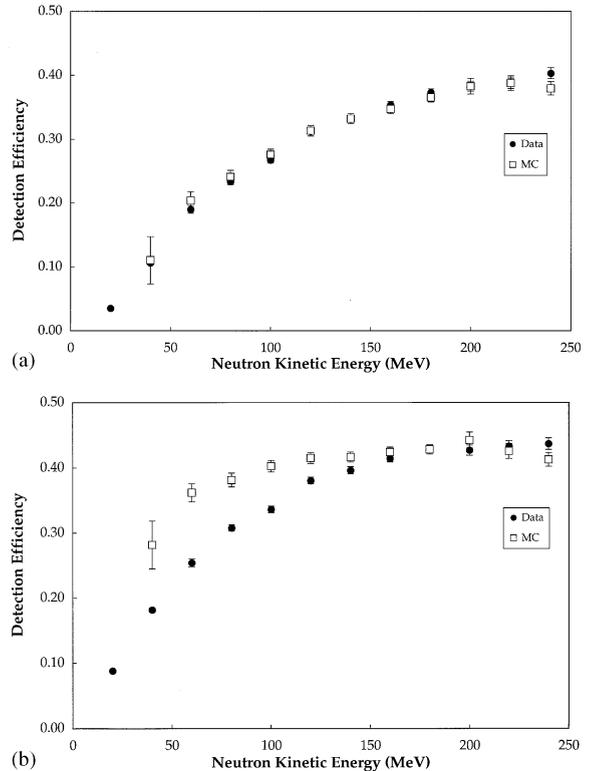

Fig. 7. (a) The neutron detection efficiency obtained from data and from Monte Carlo is displayed as a function of the neutron energy incident on the NaI, with a 20 MeV cluster energy threshold used in the analysis. The Monte Carlo events were simulated using the FLUKA/GHEISHA codes in GEANT. The neutral-hadron cutoff was set to 2 MeV in the Monte Carlo. (b) The same plot as in Fig. 7a except that a 10 MeV cluster energy threshold was used in the analysis.

neutron-induced clusters, satisfying the cluster threshold energy cut and angle cuts described above, divided by the total number of CEX reactions in our sample for which the neutron could have been detected. This neutron detection efficiency as determined from our data is shown as a function of the incident neutron energy in Fig. 7a (Fig. 7b) for a cluster threshold-energy of 20 MeV (10 MeV) and is tabulated in Table 2. The errors given are statistical errors only. We estimate a 1–2% systematic uncertainty in the energy-dependent neutron detection efficiency attributed to uncertainties in the estimated neutron energy and to the cuts imposed. A mis-estimation of the neutron energy, as determined from the measured π° and the two-body kinematics will have little effect on the reported neutron detection efficiencies at the higher neutron energies because the efficiency is nearly flat in this region. The systematic effects due to the choice of the cuts on the π° and the neutron mass were estimated by

altering the cuts by as much as 50% each. The net effect of these altered cuts was to change the average neutron detection efficiency by less than 1% of the measured value.

The observed reduced efficiency at low neutron energies is likely due to the lower probability that a neutron interaction will deposit sufficient energy in a single crystal so as to exceed the requisite 20-MeV (10-MeV) threshold energy. As the incident neutron energy increases, the probability of an interaction depositing energy in a crystal above the threshold energy increases. However, as the neutron energy increases, the probability that the neutron will traverse the NaI crystal without interaction also increases. These two competing

Table 2
Measured neutron detection efficiencies in NaI in the CB for a
20 MeV energy threshold and a 10 MeV threshold

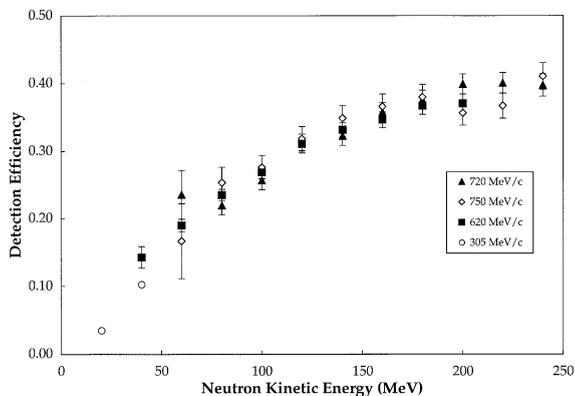| Neutron energy	20 MeV Threshold		10 MeV Threshold	
	Efficiency	σ	Efficiency	σ
20	0.035	0.002	0.088	0.002
40	0.106	0.003	0.182	0.003
60	0.189	0.006	0.254	0.006
80	0.233	0.005	0.308	0.005
100	0.267	0.005	0.336	0.005
120	0.312	0.005	0.380	0.005
140	0.333	0.005	0.396	0.005
160	0.354	0.005	0.414	0.006
180	0.373	0.006	0.428	0.006
200	0.383	0.008	0.427	0.008
220	0.388	0.008	0.433	0.008
240	0.403	0.009	0.437	0.009

Fig. 8. The neutron detection efficiency obtained from the four data sets at four momenta are shown to illustrate the internal consistency of our analysis.

effects appear to be approximately equal for the higher energy neutrons in our sample, thereby producing a plateau in the neutron detection efficiency between 35% and 40% as seen in Fig. 7.

In Fig. 8, we show the neutron detection efficiencies obtained from the four different data sets at four different π^- beam momenta, indicating good agreement between the data sets used to obtain the overall neutron detection efficiencies shown in Fig. 7.

5. The Monte Carlo simulation

In our GEANT-based Monte Carlo simulation, particles were propagated through the detector, simulating their interactions in the NaI crystals. For the electromagnetic interactions, GEANT used the EGS4 simulation code [10]. In Fig. 9, the number of crystals per cluster in the CB for photon showers in the data is compared with the same quantity obtained from the GEANT simulation. The agreement between these distributions worsened as the EGS4 cutoff energy for the photon showers was increased, requiring us to use a low cutoff energy (10 keV). (The "cutoff energy" in EGS4 is that energy at which EGS4 will cease to follow a particle and will, at that location, deposit all of the remaining particle energy.) Using
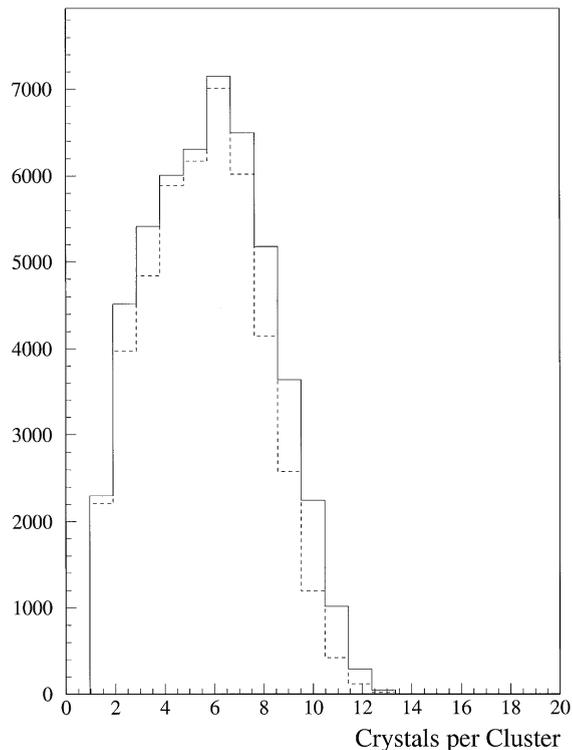

Fig. 9. The multiplicity distribution of crystals per cluster is given for photon interactions in NaI as measured with CEX events in our data. For comparison, the same quantity is shown for the GEANT simulation of photon interactions from CEX events as the dashed line. The agreement is a good one.

a low cutoff energy caused the Monte Carlo simulations to be CPU intensive.

For the neutron interactions in NaI, we tested several simulation codes. In GEANT, the default neutral hadron simulation code is called GHEISHA [11]. We found that we were unable to achieve satisfactory agreement with data by using this code alone. If, however, we used FLUKA [12] for neutrons above 20 MeV, and GHEISHA for neutrons below 20 MeV, much better agreement was achieved. We also studied two other combinations: GCALOR/MICAP (neutrons above/below 20 MeV), and FLUKA/MICAP (neutrons above/below 20 MeV) [13,14]. Overall, these latter two combinations produced less favorable agreement between data and simulation than the FLUKA/GHEISHA combination.

In Fig. 7a (Fig. 7b), we show the neutron detection efficiency for a threshold of 20 MeV (10 MeV) in our analysis. The Monte Carlo events were generated by using a neutral-hadron cutoff energy of 2.0 MeV in FLUKA/GHEISHA, a value that was found to produce the optimal agreement between the data and the Monte Carlo efficiencies. (The "neutral hadron cutoff energy" is that energy at which the neutron simulation code ceases to follow the neutron and deposits all of its remaining energy at that location.) Smaller values of this neutral-hadron cutoff energy caused the neutron detection efficiency for Monte Carlo generated events to decrease systematically at all neutron incident energies, thereby moving the Monte Carlo efficiencies below those obtained from the data at all but the lowest neutron energies. While the agreement between the data and the Monte Carlo in Fig. 7a is remarkably good, we regard this as rather fortuitous and not a reflection of the physics agreement between the simulation and the data. It is seen, for example, in Fig. 7b that the agreement at low neutron incident energies becomes dramatically worse when a cluster-energy threshold of 10 MeV is used instead of 20 MeV (Fig. 7a). One implication is that there is a small residual energy deposited in the neutron cluster in the Monte Carlo simulation that has relatively little effect on the overall efficiency for neutrons of higher energy, but which is seen to affect the efficiency from the simulation dramatically as the neutron energy is

reduced. In fact, this "excess energy" was observed in the FLUKA/GHEISHA neutron simulations which we performed and its origin is not understood at this time.

6. Neutron interaction characteristics

For those neutrons which we detected in the CB, we have plotted in Fig. 10 the measured energy in the neutron cluster versus the neutron energy predicted by the two-body kinematics. It is evident that most of the events have considerably less measured energy than that predicted, implying that not all of the neutron energy was contained in the cluster. This energy inefficiency is understood in terms of processes such as neutron scattering in which the neutron leaves the cluster
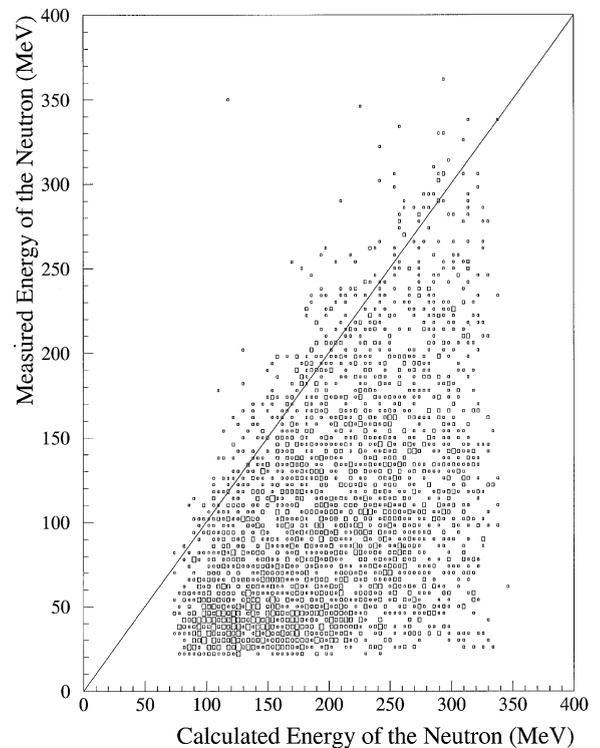

Fig. 10. The neutron detected energy is plotted versus the calculated neutron energy computed from the two-body kinematics for the CEX reaction. A general energy inefficiency is evident and is discussed in the text.

with a sizable fraction of the incident energy. We also note that, because the energy calibration of the NaI crystals was done with photon-induced showers and not with hadronic-induced showers, some disagreement between the predicted neutron energy and the energy measured may be expected.

In Fig. 10, we also see some events that lie above the equal-energy line, i.e., the detected neutron energy exceeds the neutron energy obtained by kinematics. The band of events which lie above, but near the equal-energy line reflects energy measurement fluctuations, also observed in our simulations. The few events far from the equal
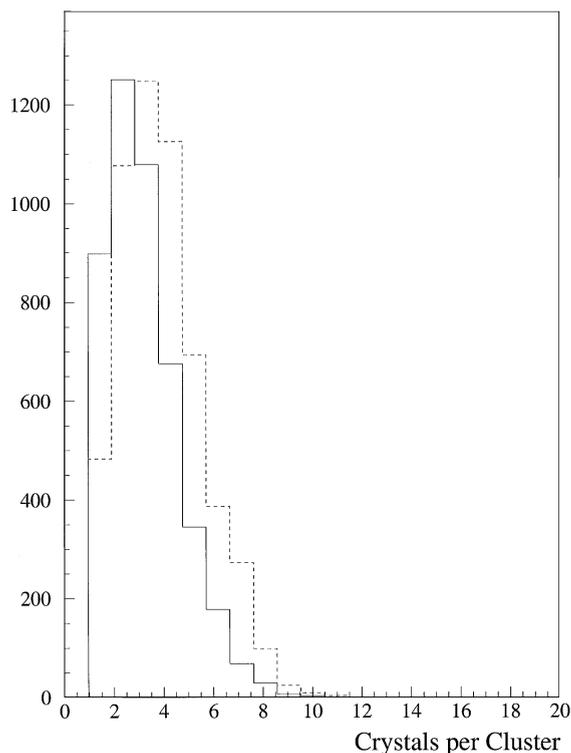

Fig. 11. We show the crystal multiplicity per cluster for neutron-induced events as measured in our CEX data as the solid line, and as simulated CEX events in the GEANT Monte Carlo with the FLUKA/GHEISHA neutron simulation codes as the dashed line. There is a systematic shift of one crystal per cluster on average placing the Monte Carlo multiplicities higher than those from the data. Moreover, the agreement depends on the choice of the neutral-hadron cutoff energy.

energy line may reflect the small background in our sample noted earlier.

In Fig. 11, we show the crystal multiplicity per cluster for neutron-induced events as measured in our data and as simulated in GEANT with the FLUKA/GHEISHA neutron simulation codes. In both plots, we have imposed a 20 MeV cluster energy threshold. The agreement between these distributions, however, depends on the choice of the neutral-hadron cutoff energy which here is 2.0 MeV, and for which we observe a systematic shift of 1 crystal per cluster higher for the Monte Carlo than for the data. To investigate whether this disagreement is a function of the neutron energy, we made comparable plots of the crystal multiplicity for the data and the Monte Carlo with neutrons selected in 50 MeV bins across our neutron energy spectrum. The larger crystal multiplicity in the Monte Carlo, seen in Fig. 11, is observed in each neutron energy bin, indicating that this disagreement is not a function of the neutron energy.

7. Discussion and conclusions

We have measured the neutron detection efficiency in the CB NaI detector for neutrons in the range 30–250 MeV incident energy under the conditions described above. In addition, we have reported on the features of the neutron interaction in the adjacent NaI crystals forming clusters of energized crystals.

A previous measurement of neutron detection efficiencies in a NaI detector system was reported by Dunphy et al. [15,16]. The overall shape of their efficiency curve is very much the same as the ones we show in Fig. 7. However, for comparable incident neutron energies, their reported neutron detection efficiencies are $\sim 20\%$ larger than those we have measured. We believe this difference can be understood in terms of the geometry of the NaI detectors in the two experiments. In both experiments, a threshold of 10 MeV was used. However, in the case of Dunphy et al., a large fraction of the hadron-induced shower is contained in their NaI crystal(s) used for the 10-MeV threshold discrimination. In the CB, the 10-MeV threshold is applied

to only one NaI crystal which is smaller than the Dunphy et al. crystals, and, because of that, it will contain a smaller fraction of the equivalent shower. This difference in shower containment implies a higher effective threshold for our measurement and therefore a decreased efficiency for observing the neutron interaction. Dunphy et al., show the effect on the measured neutron detection efficiency when only 1/3 of their detector is used with the same 10 MeV threshold, resulting in an efficiency $\sim 1/3$ of that with the full detector. We believe that our results are not in disagreement with those of Dunphy et al.

The CEX reaction was selected for this analysis because the two-body kinematics provide an unambiguously clear separation between clusters induced by photon electromagnetic showers and those induced by neutron-hadronic showers. Such distinctions are not easily made for more complicated final states involving as many as six or more clusters in the CB detector. Efforts have been underway to attempt to separate the neutron-induced clusters from the photon-induced clusters, but the results are at present inconclusive. A reliable Monte Carlo simulation can be helpful in this study.

Finally, it appears clear from Figs. 7a and 7b that experiments performed with neutrons whose kinetic energies are below 100 MeV will find it increasingly more difficult to detect the neutron in NaI as the neutron energy decreases. Moreover, based on the Monte Carlo packages used in our studies, the simulation of the behavior of neutrons in the NaI becomes less accurate at low neutron energies.

References

[1] M. Oreglia et al., Phys. Rev. D 25 (1982) 2259.
[2] Y. Chan et al., IEEE Trans. Nucl. Sci. NS-25 (1978) 333.
[3] E.D. Bloom, C.W. Peck, Ann. Rev. Nucl. Sci. 33 (1983) 143.
[4] J.E. Gaiser et al., Phys. Rev. D 34 (1986) 711.
[5] D. Antreasyan et al., Phys. Rev. D 36 (1987) 2633.
[6] D.A. Williams et al., Phys. Rev. D 38 (1988) 1365.
[7] H. Marsiske et al., Phys. Rev. D 41 (1990) 3324.
[8] A. Bizzeti et al., Phys. Lett. B 267 (1991) 286.
[9] GEANT version 3.21; CERN Program Library Long Writeup W5013; URL: http://wwwinfo.cern.ch/asdoc/geant_html13/geantall.html.
[10] EGS4: W.R. Nelson, H. Hirayama, D.W.O. Rogers, The EGS4 Code System, Stanford Linear Accelerator Center Report SLAC-265, 1985.
[11] The GEANT/GHEISHA Interface, GEANT Manual, PHYS510-1.
[12] The GEANT/FLUKA Interface, GEANT Manual, PHYS520-1
[13] GCALOR: C. Zeitnitz, T.A. Gabriel, Proceedings of the International Conference on Calorimetry in High Energy Physics, Tallahassee, FL, USA, February 1993, p. 376.
[14] The GEANT/MICAP Interface, GEANT Manual, PHYS530-1
[15] P.P. Dunphy et al., Expt. Astr. 2 (1992) 233.
[16] P.P. Dunphy et al., Nuclear Inst. and Meth. A 330 (1993) 199.